Pergamon

Int. J. Heat Mass Transfer. Vol. 41, No. 11, pp. 1513–1529, 1998

Printed in Great Britain
0017-9310/98 $19.00+0.00

PII: S0017-9310(97)00216-0

A Galerkin finite-element study of the onset of double-diffusive convection in an inclined porous enclosure

M. MAMOU, P. VASSEUR and E. BILGEN

Ecole Polytechnique, University of Montreal, C.P. 6079 Succ 'Down Town' Montreal, PQ, Canada, H3C 3A7

(*Received* 27 *November* 1996 *and in final form* 14 *July* 1997)

Abstract—The Darcy model with the Boussinesq approximation is used to study the onset of double-diffusive natural convection in an inclined porous cavity. Transverse gradients of heat and solute are applied on two opposing walls of the cavity, while the other two walls are impermeable and adiabatic. The analysis deals with the particular situation where the buoyancy forces induced by the thermal and solutal effects are opposing and of equal intensity. The objective of this study is to investigate the critical stability of this system in terms of the inclination angle, the aspect ratio of the cavity and the Lewis number. The subsequent behavior of the convective flow is also discussed in terms of the governing parameters of the problem. Numerical procedures based on the Galerkin and finite element methods are carried out to investigate the onset of double-diffusive convection using the linear stability analysis. It is shown that for values of Lewis number around unit, overstability is possible provided that the normalized porosity of the porous medium ε is made smaller than unity. For supercritical convection, the occurrence of multiple solutions, for a given range of the governing parameters, is demonstrated. The numerical results also indicate the existence of subcritical convective regimes. © 1998 Elsevier Science Ltd. All rights reserved.

INTRODUCTION

Natural convection heat transfer through porous media has been studied extensively in the past, owing to relevance in many natural and industrial problems. A recent review of the literature [1] indicates that the bulk of the research effort has been devoted to flows induced by a single buoyancy force, namely temperature gradients. Recently, interest for flows resulting from the combined action of both temperature and concentration has surged in view of its fundamental importance in various engineering problems. Prominent among these are the migration of moisture contained in fibrous insulation, grain storage, the transport of contaminants in saturated oil, the underground disposal of nuclear wastes, drying processes, etc.

Natural convection induced by the variation of both temperature and concentration gradients, the so-called double diffusion flow or combined heat and mass transfer flow, often exhibits special features that lack counterparts in flows driven by a single buoyancy effect. This follows from the fact that heat and solute diffuse at different rates such that complex flow structures may be expected. Relative to the research activity on buoyancy flows driven by a single buoyancy effect, the work on double-diffusion in porous media primarily focused on the onset of convection in a horizontal layer heated and salted from below [2–5]. On the basis of a linear stability analysis, criteria for the onset of motion, via stationary and oscillatory modes, were derived for various conditions. Finite amplitude convection in a square cavity heated from below has been investigated numerically by Rosenberg and Spera [6] for a variety of boundary and initial conditions on the salinity field. The flow dynamics were found to depend strongly on the solutal to thermal buoyancy ratio N. Double-diffusive convection in a horizontal porous layer has been considered by Chen and Chen [7] on the basis of the Darcy equation, including Brinkman and Forchheimer terms. The stability boundaries which separate regions of different types of convective motion (steady, periodic and unsteady) were numerically identified in terms of thermal and solute Rayleigh numbers.

Available studies with double-diffusive natural convection in confined porous media are concerned mostly with rectangular cavities submitted to horizontal temperature and concentration gradients [8]. The cases of both the augmenting double-diffusion, where the flow is driven in the same direction by the thermal and solutal forces, and the counteracting convection, where the flow is driven in opposite directions by the two driving forces, have been investigated and contrasted. In the case of augmenting double-diffusion, Trevisan and Bejan [8] completed an analytical and numerical study relative to heat and mass transport processes through a vertical porous layer subject to uniform fluxes of heat and mass from the side. Their results, valid only for the case $Le = 1$, were extended by Alavyoon [9] and Mamou *et al.* [10], using the parallel flow approximation, to account for

NOMENCLATURE

A aspect ratio, H'/W'
D solutal diffusivity
g acceleration due to gravity
H' height of the enclosure
K permeability of the porous medium
k thermal conductivity of the saturated porous medium
Le Lewis number, α/D
m total number of nodes, $m=(2N_{ex}+1)\times(2N_{ey}+1)$
N^e total number of elements, $N_{ex}\times N_{ey}$
N_{ex} number of elements in x-direction
N_{ey} number of elements in y-direction
N buoyancy ratio, $\beta_S\Delta S'/\beta_T\Delta T'$
Nu Nusselt number, eqn (14)
R_S solutal Darcy–Rayleigh number, $g\beta K\Delta S'W'/D\nu$
R_T thermal Darcy–Rayleigh number, $g\beta K\Delta T'W'/\alpha\nu$
R_{TC} critical thermal Rayleigh number
R^0 constant, eqn (34)
R_T^0 normalized thermal Darcy–Rayleigh number, $R_T/|R^0|$
S dimensionless concentration, $(S'-S_0')/\Delta S'$
S_H' higher concentration of the hot wall
S_L' lower concentration of the cold wall
S_0' reference concentration, $S_0'=(S_H'+S_L')/2$
$\Delta S'$ characteristic concentration, $S_H'-S_L'$
Sh Sherwood number, eqn (14)
T dimensionless temperature, $(T'-T_0')/\Delta T'$
T_H' temperature of the hot wall
T_L' temperature of the cold wall
T_0' reference temperature, $T_0'=(T_H'+T_L')/2$
$\Delta T'$ characteristic temperature, $T_H'-T_L'$
t dimensionless time, $t'\alpha/(\sigma W'^2)$
u, v dimensionless velocities in x- and y-directions, $(u', v')W'/\alpha$
W' width of the enclosure
x, y coordinate system, $(x', y')/W'$.

Greek symbols
α thermal diffusivity $(k/(\rho c)_f)$
β_S solutal expansion coefficient
β_T thermal expansion coefficient
ε normalized porosity of the porous medium, $\varepsilon=\phi/\sigma$
λ eigenvalue
ν kinematic viscosity of fluid
ρ density of fluid
$(\rho c)_f$ heat capacity of fluid
$(\rho c)_p$ heat capacity of saturated porous medium
σ heat capacity ratio, $(\rho c)_p/(\rho c)_f$
ϕ porosity of the porous medium
Ψ dimensionless stream function, Ψ'/α.

Superscripts
$[\,]^{-1}$ inverse of a matrix
$'$ dimensional variable.

Subscripts
C pure diffusive state
max maximum value
min minimum value.

Operators
$\mathcal{F}(f) = \sin\Phi\,(\partial f/\partial x)+\cos\Phi\,(\partial f/\partial y)$
$J(f,g) = [(\partial f/\partial y)(\partial g/\partial x)]-[(\partial f/\partial x)(\partial g/\partial y)]$.

the case of $Le\neq 1$ and the inclination of the enclosure, respectively. The Nusselt and Sherwood numbers, predicted by these authors, were found to be in good agreement with numerical solutions for a large range of the governing parameters. The case of natural convection in a porous enclosure, due to opposing buoyancy forces, has also been considered recently [11–13]. Of particular interest is the flow regime occurring when $N\simeq -1$. For this situation, the most striking effect is the very weak convection resulting from the fact that the buoyancy forces are comparable in size but have opposite signs [10, 11]. In this limit the existence of oscillating convection has been reported by Alavyoon *et al.* [12]. Also, as demonstrated analytically and numerically by Mamou *et al.* [10, 13], multiple patterns of convection are possible for a given range of the governing parameters. Recently, Mamou *et al.* [14] considered the problem of a tall porous cavity, subject to constant fluxes of heat and mass on its long side walls. Their attention was focused on the particular situation where the opposing buoyancy forces are of equal intensity ($N=-1$). It was demonstrated analytically that there exists a critical Rayleigh number below which the fluid remains at rest. Above this critical value, their analytical results show that two convective solutions (one stable and the other unstable) bifurcate from the rest state.

The peculiar behavior of double-diffusive convection occurring when $N=-1$ motivates the present study. The specific problem considered here is the study of the onset of double-diffusive convection within an inclined cavity, when the thermal and solutal buoyancy forces are equal and in opposite direction. In the following sections the mathematical for-

mulation for the problem is first given. Then, a numerical linear stability analysis is performed to investigate the onset of motion. Subsequently, a numerical simulation of the full governing equations is carried out to study the flow and heat transfer rates at supercritical Rayleigh numbers. Finally, the results from the numerical computations are discussed in detail.

PROBLEM DESCRIPTION AND MATHEMATICAL MODEL

The system considered in this study is the two-dimensional inclined rectangular porous cavity shown in Fig. 1(a). The enclosure is of height H', width W' and is tilted at an angle Φ with respect to the horizontal plane. The wall at $x' = -W'/2$ represents the low-temperature (T'_L) and low-concentration (S'_L) boundary, and the wall at $x' = W'/2$ denotes the high-temperature (T'_H) and high concentration (S'_L) boundary. The other two walls are regarded as being insulated and impermeable. The fluid saturated porous medium is assumed homogeneous and isotropic and inertial effects are neglected. The solution that saturates the porous matrix is modeled as a Boussinesq incompressible fluid whose density variation can be expressed as

$$\rho = \rho_0[1-\beta_T(T'-T'_0)-\beta_S(S'-S'_0)] \qquad (1)$$

where β_T and β_S are the thermal and concentration

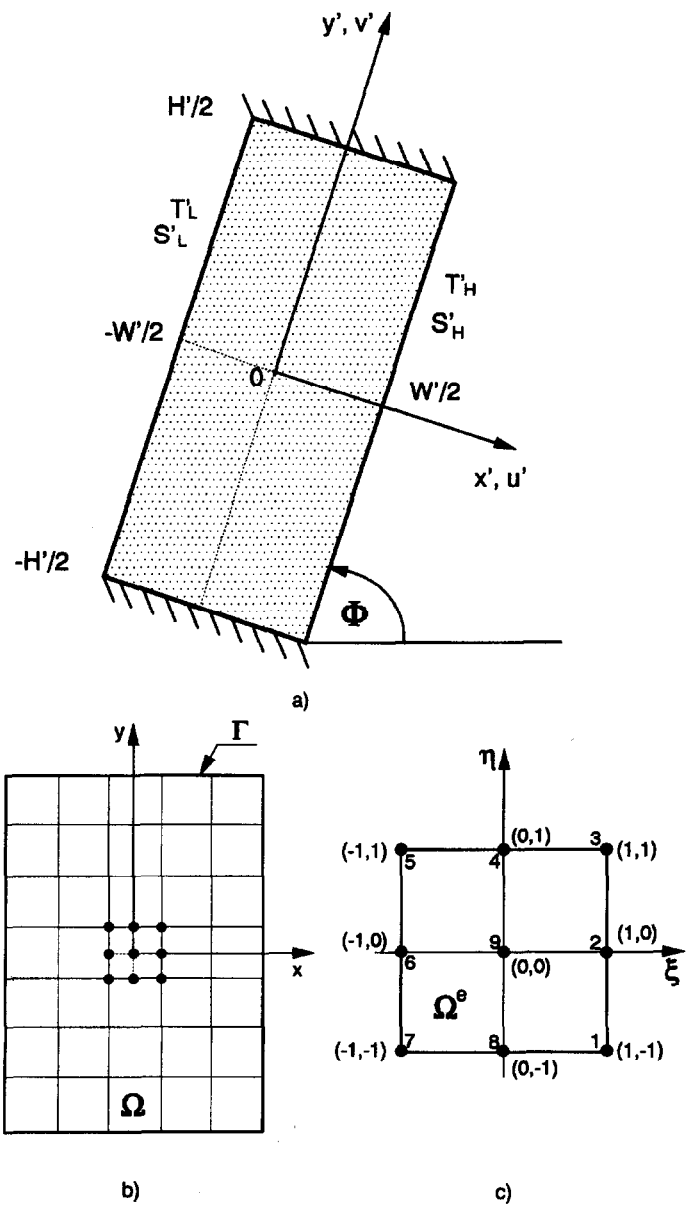

Fig. 1. (a) Geometry of the problem; (b) finite element mesh; (c) nine-node Lagrangian element.

expansion coefficients. Subscript 0 stands for a reference state.

The equations governing the conservation of momentum, energy and constituent in the solution-saturated porous medium are (see for instance Mamou *et al.* [10])

$$\nabla^2\Psi = -R_T\mathscr{F}(T+NS) \tag{2}$$

$$\frac{\partial T}{\partial t}+J(\Psi,T)=\nabla^2 T \tag{3}$$

$$\varepsilon\frac{\partial S}{\partial t}+J(\Psi,S)=Le^{-1}\nabla^2 S \tag{4}$$

where the operators $\mathscr{F}$ and J are defined in the nomenclature and Ψ is the stream function, given by

$$u=\frac{\partial\Psi}{\partial y}\quad v=-\frac{\partial\Psi}{\partial x} \tag{5}$$

such that the continuity equation is automatically satisfied.

The above equations were nondimensionalized by introducing the following variables

$$\left.\begin{aligned}(x,y)&=\left(\frac{x}{W'},\frac{y'}{W'}\right)\\(u,v,\psi)&=\left(u'\frac{W'}{\alpha},v'\frac{W'}{\alpha},\frac{\psi'}{\alpha}\right)\\t&=t'\frac{\alpha}{\sigma W'^2}\\T&=\frac{T'-T'_0}{\Delta T'}\\\Delta T'&=T'_H-T'_L\\T'_0&=\frac{T'_H+T'_L}{2}\\S&=\frac{S'-S'_0}{\Delta S'}\\\Delta S'&=S'_H-S'_L\\S'_0&=\frac{S'_H+S'_L}{2}\end{aligned}\right\} \tag{6}$$

where u' and v' are the volume-averaged velocity components, T' and S' the temperature and the concentration of the constituent, t' is the time, α is the thermal diffusivity of the porous medium, σ is the saturated porous medium to fluid heat capacity ratio, and $\varepsilon=\phi/\sigma$ is the normalized porosity of the porous matrix.

The dimensionless boundary conditions sketched in Fig. 1 are expressed by

$$\left.\begin{aligned}x=\pm\tfrac{1}{2}\quad&\Psi=0\quad T=S=\pm\tfrac{1}{2}\\y=\pm\frac{A}{2}\quad&\Psi=0\quad\frac{\partial T}{\partial y}=\frac{\partial S}{\partial y}=0\end{aligned}\right\} \tag{7}$$

The non-dimensionalization process results in the appearance of six dimensionless parameters in the governing equations and boundary conditions, namely the thermal Darcy–Rayleigh number R_T, the solutal to thermal buoyancy ratio N, the Lewis number Le, the cavity aspect ratio A, the normalized porosity ε and the inclination angle of the cavity Φ, defined as

$$R_T=\frac{g\beta_T K\Delta T' W'}{\alpha\nu}\quad N=\frac{\beta_S\Delta S'}{\beta_T\Delta T'}$$

$$Le=\frac{\alpha}{D}\quad\varepsilon=\frac{\phi}{\sigma}\quad A=\frac{H'}{W'} \tag{8}$$

where K is the permeability of the porous medium and D the mass diffusivity through the fluid mixture.

It is noted that the volumetric expansion coefficient due to temperature change, defined as $\beta_T=-(1/\rho_0)(\partial\rho/\partial T')$ is normally positive, but the volumetric expansion coefficient for concentration, defined as $\beta_S=-(1/\rho_0)(\partial\rho/\partial S')$ can be either positive ($N>0$) or negative ($N<0$). For the boundary conditions prescribed by eqn (7) it is clear that a positive value of N results in augmenting convection, since the temperature-induced buoyancy is along the same direction as the solute-induced buoyancy. In contrast, when N is negative it is expected that the resulting convection will be considerably weakened by the counteracting thermal and solutal buoyancy forces.

The foregoing analysis is concerned with the special case $N=-1$ for which the thermal and solutal buoyancy forces are equal and opposite. For this situation, it is clear that a rest state ($\Psi=0$), where heat and mass are being transferred via pure diffusion, is a possible solution for the steady state form of eqns (2)–(4) and (7). Whether or not this no-flow solution will remain stable, regardless of how high a R_T is imposed, has to be determined by a stability analysis. In this context, it is convenient to consider the pure diffusive solution as a part of the total solution. Thus, we introduce the following transformation

$$\left.\begin{aligned}\Psi&=\Psi_C+\dot\psi(t,x,y)\\T&=T_C+\dot\theta(t,x,y)\\S&=S_C+\dot\phi(t,x,y)\end{aligned}\right\} \tag{9}$$

where the static state of the system is characterized by

$$\Psi_C=0\quad T_C=S_C=x \tag{10}$$

Substituting the above expressions into eqns (2)–(4) and making $N=-1$ yields the following system of governing equations

$$\nabla^2\dot\psi=-R_T\mathscr{F}(\dot\theta-\dot\phi) \tag{11}$$

$$\frac{\partial\dot\theta}{\partial t}+\frac{\partial\dot\psi}{\partial y}+J(\dot\psi,\dot\theta)=\nabla^2\dot\theta \tag{12}$$

$$\varepsilon\frac{\partial\dot\phi}{\partial t}+\frac{\partial\dot\psi}{\partial y}+J(\dot\psi,\dot\phi)=Le^{-1}\nabla^2\dot\phi \tag{13}$$

The heat and mass transfer rates across the system can be expressed by the overall Nusselt (Nu) and Sherwood (Sh) numbers which are important in engineering applications. They are, respectively, defined as

$$\left.\begin{aligned} Nu &= \frac{1}{A}\int_{-A/2}^{A/2} \left.\frac{\partial T}{\partial x}\right|_{x=\pm 1/2} \mathrm{d}y \\ Sh &= \frac{1}{A}\int_{-A/2}^{A/2} \left.\frac{\partial S}{\partial x}\right|_{x=\pm 1/2} \mathrm{d}y \end{aligned}\right\} \tag{14}$$

LINEAR STABILITY ANALYSIS

In this section, the physical situation described by eqns (11)–(13) is examined from the standpoint of stability to small perturbations from the equilibrium state.

As usual, the functions $\dot{\psi}$, $\dot{\theta}$ and $\dot{\varphi}$ are expanded in their normal modes, assuming separability, in the following way

$$\left.\begin{aligned} \dot{\psi}(t,x,y) &= e^{pt}\psi(x,y) \\ \dot{\theta}(t,x,y) &= e^{pt}\theta(x,y) \\ \dot{\varphi}(t,x,y) &= e^{pt}\varphi(x,y) \end{aligned}\right\} \tag{15}$$

where p is the growth rate of the perturbation.

Introducing the above functions into eqns (11)–(13), dropping second higher-order non-linear terms in the perturbations, one obtain the following set of linearized equations

$$\nabla^2\psi = -R_T\mathscr{F}(\theta-\varphi) \tag{16}$$

$$p\theta + \frac{\partial\psi}{\partial y} = \nabla^2\theta \tag{17}$$

$$\varepsilon p\varphi + \frac{\partial\psi}{\partial y} = Le^{-1}\nabla^2\varphi \tag{18}$$

with the boundary conditions

$$\left.\begin{aligned} x &= \pm\tfrac{1}{2} \quad \psi = \theta = \varphi = 0 \\ y &= \pm\frac{A}{2} \quad \psi = \frac{\partial\theta}{\partial y} = \frac{\partial\varphi}{\partial y} = 0 \end{aligned}\right\} \tag{19}$$

In general, the solution of eqns (16)–(18) is not limited to a single Fourier component in either x or y-direction and therefore an analytical process can be tedious. For this reason, the Galerkin finite element method is used to solve the above linear system of equations.

Using the Green theorem, the variational formulation of eqns (16)–(18) yields the following Galerkin integrals

$$\int_\Omega \nabla\psi\cdot\nabla w\,\mathrm{d}\Omega - \int_\Gamma \frac{\partial\psi}{\partial n} w\,\mathrm{d}\Gamma = \int_\Omega R_T\mathscr{F}(\theta-\varphi)w\,\mathrm{d}\Omega \tag{20}$$

$$\int_\Omega p\theta\vartheta\,\mathrm{d}\Omega + \int_\Omega \frac{\partial\psi}{\partial y}\vartheta\,\mathrm{d}\Omega = -\int_\Omega \nabla\theta\cdot\nabla\vartheta\,\mathrm{d}\Omega + \int_\Gamma \frac{\partial\theta}{\partial\mathbf{n}}\vartheta\,\mathrm{d}\Gamma \tag{21}$$

$$\int_\Omega \varepsilon p\varphi\vartheta\,\mathrm{d}\Omega + \int_\Omega \frac{\partial\psi}{\partial y}\vartheta\,\mathrm{d}\Omega = -\int_\Omega Le^{-1}\nabla\varphi\cdot\nabla\vartheta\,\mathrm{d}\Omega + \int_\Gamma Le^{-1}\frac{\partial\varphi}{\partial\mathbf{n}}\vartheta\,\mathrm{d}\Gamma \tag{22}$$

where $\mathbf{n}$ is the outward-oriented normal vector, $\mathrm{d}\Gamma$ is the infinitesimal portion length of the boundary $\partial\Omega = \Gamma$, w and ϑ are the shape functions satisfying the boundary conditions in eqn (19). According to the boundary condition of ψ, θ and φ, the boundary integrals ($\int_\Gamma$) in eqns (20)–(22) known as the natural boundary conditions are nil (for more detail see Ref. [15]).

In the following sections the conditions for stationary instability will be first discussed. Then, the boundary for oscillatory instability will be delineated.

Instability via stationary convection $\mathrm{p} = 0$: *finite element method*

We consider here the marginal state of stability via stationary convection, for which the exchange of stability is valid.

The Bubnov–Galerkin procedure based on the nine-noded biquadratic rectangular elements (see Fig. 1b–c) was used to discretize the perturbed governing eqns (20)–(22). In each element, the unknown variables (i.e. ψ, θ and φ) are approximated by the following expansions

$$\begin{Bmatrix}\psi\\ \theta\\ \varphi\end{Bmatrix} \simeq \sum_{j=1}^{9} \Theta_j(x,y)\begin{Bmatrix}\psi_j\\ \theta_j\\ \varphi_j\end{Bmatrix} \tag{23}$$

where $\Theta_j(x,y)$ are the Lagrangian shape functions (Norrie and Vries [16]), while ψ_j, θ_j and φ_j are nodal values.

For each element, the numerical procedure yields the element matrix equations. After assemblage of all the element matrices into the global matrices, one can obtain the following systems of space-discretized equations (see [16, 17])

$$[K_\psi]\{\psi\} = R_T[B]\{\theta-\varphi\} \tag{24}$$

$$[L]\{\psi\} = [K]\{\theta\} \tag{25}$$

$$[L]\{\psi\} = Le^{-1}[K]\{\varphi\} \tag{26}$$

where $[B]$, $[K_\psi]$, $[K]$ and $[L]$ are $m\times m$ square matrices whose components are functions of the orientation angle Φ and the aspect ratio A of the cavity; $m = (2N_{ex}+1)\times(2N_{cy}+1)$ is the total number of nodes in the discretized domain.

Specifically, these matrices are defined by

$$\left.\begin{aligned}[B] &= \int_\Omega \mathscr{F}(\Theta_j)\Theta_i \,d\Omega \qquad [L] = -\int_\Omega \frac{\partial \Theta_j}{\partial y}\Theta_i \,d\Omega \\ [K_\psi] &= \int_\Omega \nabla\Theta_j \cdot \nabla\Theta_i \,d\Omega \qquad [K] = \int_\Omega \nabla\Theta_j \cdot \nabla\Theta_i \,d\Omega\end{aligned}\right\} \tag{27}$$

The above integrals are evaluated by the use of the Gauss integration formulae. It is noted that, upon introducing the boundary conditions from eqn (19), the matrices $[K_\psi]$ and $[K]$ become different from each other. The Dirichlet boundary conditions in eqn (19) are introduced in the above systems of equations without altering the size of the matrices. In eqn (24), if i is the subscript of a known nodal value of ψ_i on Γ the ith row and the ith column of $[K_\psi]$ are set equal to zero and $[K_\psi]_{i,i}$ is set equal to unity. On the other hand the ith row of $[B]$ is set equal to zero. The same technique is applied for eqns (25) and (26). An outline of the procedure used here is given by Norrie and Vries [16] and Huebner *et al.* [17].

From eqns (25) and (26) it is clear that $\{\varphi\} = Le\{\theta\}$ such that the linear system of eqns (24)–(26) reduces to

$$R_T(1-Le)[E]\{\psi\} - \{\psi\} = 0 \tag{28}$$

where $[E]$ is an $m \times m$ square matrix defined as $[E] = [K_\psi]^{-1}[B][K]^{-1}[L]$.

The above equation can be rearranged to the following canonical form

$$[[E] - \lambda[\mathbf{I}]]\{\psi\} = 0 \tag{29}$$

where $\mathbf{I}$ is the identity matrix, λ is the eigenvalue defined such that

$$R_T(1-Le) = \frac{1}{\lambda} \tag{30}$$

and $\{\psi\}$ is the eigenvector.

To perform the required matrix algebra, computations were carried out on an IBM 9000 using double precision subroutines of the IMSL library. The solution of eqn (29) gives m eigenvalues of $[E]$ and the corresponding stream function fields. The temperature $\{\theta\}$ and concentration $\{\varphi\}$ fields are then obtained from eqns (25) and (26) as

$$\{\theta\} = [K]^{-1}[L]\{\psi\} \qquad \{\varphi\} = Le[K]^{-1}[L]\{\psi\} \tag{31}$$

The eigenvalues of (29), can be rearranged as follows

$$\{\lambda\} = (\lambda_1, \lambda_2, \ldots, \lambda_m) \tag{32}$$

such that

$$\lambda_1 \leqslant \lambda_2 \leqslant \cdots \leqslant \lambda_{m-1} \leqslant \lambda_m \tag{33}$$

Then, the supercritical Rayleigh number for the onset of motion can be obtained from

$$R_{TC} = \frac{R^0}{(1-Le)} \tag{34}$$

where R^0 is a constant depending only on the inclination angle Φ and the aspect ratio A of the cavity. It can be shown that

$$\left.\begin{aligned}R^0 &= \frac{1}{\lambda_1}, \quad \text{when } Le > 1 \\ R^0 &= \frac{1}{\lambda_m}, \quad \text{when } Le < 1\end{aligned}\right\} \tag{35}$$

From eqn (34) it is clear that when $Le \to 1$, the critical Rayleigh number for the onset of motion tends towards infinity.

For a square cavity ($A = 1$), the computed values of R^0 are given in Table 1 for various inclination angles Φ.

The precision of the value of the critical Rayleigh number predicted by the present numerical procedure depends on the grid numbers ($N_{ex} \times N_{ey}$). Numerical tests, using various mesh sizes were done for the same conditions in order to determine the best compromise between accuracy of the results and computing time. Typical results are presented in Table 2 for the case of a horizontal square cavity (i.e. $\Phi = 0°$ and $A = 1$), for which the exact value $R^0 = 4\pi^2$ has been predicted analytically in the past by Nield [2].

According to the above results, the error (%) of the computed values is found to vary linearly with h^a, where h being the mesh size and $a \simeq 4$ denoting the convergence rate of the numerical results.

Based on the above results a mesh size of 10×10 was adopted in this study for all cases dealing with ($A \simeq 1$). However, for $A \simeq 8$, a mesh size of 10×35 was required. Further decrease of the mesh size did not cause any significant change in the final results.

Instability via oscillatory convection ($p \neq 0$): *Galerkin method*

The marginal state of instability via oscillatory convection will be now discussed. Let us suppose that the perturbed stream function ψ, temperature θ and concentration φ fields are given by the following functions

Table 1. Critical Rayleigh number R^0 for $A = 1$, $\Phi = 0°$, 45° and 90° and for $N_{ex} = N_{ey} = 16$ ($m = 1089$)

$R^0 = \frac{1}{\lambda_i}$	$\Phi = 0°$	$\Phi = 45°$	$\Phi = 90°$
$i = 1$	∞	−2075.093	−184.069
$i = 2$	∞	−2161.500	−227.930
$i = 3$	∞	−3471.134	−489.868
$i = m-2$	109.695	141.929	489.868
$i = m-1$	61.688	81.920	227.930
$i = m$	39.479	53.497	184.069

Table 2. Effect of the grid size on the precision of the computed value of R^0 for ($A = 1$, $\Phi = 0°$ and $Le < 1$)

$N_{ex} \times N_{ey}$	4×4	8×8	12×12	16×16	Ref. [2]
R^0	39.5183548	39.4809956	39.4789301	39.4785801	39.47841760
Error [%]	1.01×10^{-1}	6.53×10^{-3}	1.30×10^{-3}	4.12×10^{-4}	
CPU [s]	3.9	98.1	1123.6	5830.3	

$$\left.\begin{aligned} \psi(x,y) &= \psi_0 f(x,y) \\ \theta(x,y) &= \theta_0 g(x,y) \\ \varphi(x,y) &= \varphi_0 g(x,y) \end{aligned}\right\} \tag{36}$$

where ψ_0, θ_0 and φ_0 are the amplitudes of the dynamic perturbations (ψ, θ, φ) and $f(x,y)$ and $g(x,y)$ are space functions satisfying the boundary conditions in eqn (19). They describe the perturbed stream function, temperature and concentration fields at the onset of convection. Since the linear stability theory predicts only the size of the convective cells but says nothing about the flow intensity, the functions $f(x,y)$ and $g(x,y)$ have been normalized in such a way that $0 \leqslant |f(x,y)| \leqslant 1$ and $0 \leqslant |g(x,y)| \leqslant 1$.

Substituting eqn (36) into eqns (20)–(22) and making use of $w = f(x,y)$ and $\vartheta = g(x,y)$, yields

$$\mathscr{K}_\psi \psi_0 = R_T \mathscr{B}(\theta_0 - \varphi_0) \tag{37}$$

$$p\mathscr{M}\theta_0 - \mathscr{L}\psi_0 = -\mathscr{K}\theta_0 \tag{38}$$

$$\varepsilon \mathscr{M} p\varphi_0 - \mathscr{L}\psi_0 = -Le^{-1}\mathscr{K}\varphi_0 \tag{39}$$

where $\mathscr{B}$, $\mathscr{K}_\psi$, $\mathscr{K}$, $\mathscr{L}$ and $\mathscr{M}$ are constants which can be computed from the following integrals

$$\left.\begin{aligned} \mathscr{B} &= \int_\Omega \mathscr{F}(g) f \, d\Omega \quad \mathscr{L} = -\int_\Omega \frac{\partial f}{\partial y} g \, d\Omega \\ \mathscr{K}_\psi &= \int_\Omega (\nabla f)^2 \, d\Omega \quad \mathscr{K} = \int_\Omega (\nabla g)^2 \, d\Omega \\ \mathscr{M} &= \int_\Omega g^2 \, d\Omega \end{aligned}\right\} \tag{40}$$

For the problem considered here the functions $f(x,y)$ and $g(x,y)$ are in general difficult to be predicted analytically and they were computed numerically by the finite element model described above. Substituting $f_i(x,y)$ by ψ_i and $g_i(x,y)$ by $\theta_{i,j}$ or $\varphi_{i,j}$ and making use of eqn (27), the constants $\mathscr{B}$, $\mathscr{K}_\psi$, $\mathscr{K}$, $\mathscr{L}$ and $\mathscr{M}$ are obtained from the following expressions

$$\left.\begin{aligned} \mathscr{B} &= \sum_{k=1}^{N^e} \left(\sum_{i=1}^{9} \sum_{j=1}^{9} [B]^e_{i,j} \theta^e_j \psi^e_i \right)_k \\ \mathscr{L} &= \sum_{k=1}^{N^e} \left(\sum_{i=1}^{9} \sum_{j=1}^{9} [L]^e_{i,j} \psi^e_j \theta^e_i \right)_k \\ \mathscr{K}_\psi &= \sum_{k=1}^{N^e} \left(\sum_{i=1}^{9} \sum_{j=1}^{9} [K_\psi]^e_{i,j} \psi^e_j \psi^e_i \right)_k \\ \mathscr{K} &= \sum_{k=1}^{N^e} \left(\sum_{i=1}^{9} \sum_{j=1}^{9} [K]^e_{i,j} \theta^e_j \theta^e_i \right)_k \\ \mathscr{M} &= \sum_{k=1}^{N^e} \left(\sum_{i=1}^{9} \sum_{j=1}^{9} [M]^e_{i,j} \theta^e_j \theta^e_i \right)_k \end{aligned}\right\} \tag{41}$$

where N^e is the total number of elements over the calculus domain and the superscript e refers to a finite element in the discretized domain.

The precision of the above procedure can be assessed for the special case of an horizontal cavity ($\Phi = 0°$) for which, according to Nield's analytical solution [2], the functions $f(x,y)$ and $g(x,y)$ are given by

$$f(x,y) = \cos(\pi x)\cos(\pi y) \quad g(x,y) = \cos(\pi x)\sin(\pi y) \tag{42}$$

Substituting the above expressions into eqn (40) and performing the resulting integrals yields the following results

$$\mathscr{B} = \mathscr{L} = \frac{\pi}{4} \quad \mathscr{K}_\psi = \mathscr{K} = \frac{\pi^2}{2} \quad \mathscr{M} = \frac{1}{4} \tag{43}$$

On the other hand, for a grid (16×16) it was found numerically, from the present numerical procedure [eqn (41)], that

$$\mathscr{B} = \mathscr{L} = 0.785385 \tag{44}$$

$$\mathscr{K}_\psi = \mathscr{K} = 4.934731 \quad \mathscr{M} = 0.249996$$

which are in good agreement with the exact solution [eqn (43)]. For a square vertical cavity ($A = 1$, $\Phi = 90°$) these constants have the following values

$$\mathscr{B} = 0.706584 \quad \mathscr{L} = 0.976830$$

$$\mathscr{K}_\psi = 13.374099 \quad \mathscr{K} = 9.499478 \tag{45}$$

$$\mathscr{M} = 0.245210$$

Substituting eqns (38) and (39) into eqn (37) yields a second-order polynomial equation in terms of the growing rate p

$$p^2 - 2p_0p_1p - p_0^2p_2 = 0 \tag{46}$$

where

$$\left.\begin{aligned} p_0 &= \frac{\gamma}{2\varepsilon Le R^0} \\ p_1 &= R_T Le(\varepsilon - 1) - R^0(1 + \varepsilon Le) \\ p_2 &= 4R^0 \varepsilon Le[R_T(1 - Le) - R^0] \end{aligned}\right\} \tag{47}$$

and the constants R^0 and γ are defined by

$$R^0 = \frac{\mathscr{K}_\psi \mathscr{K}}{\mathscr{B}\mathscr{L}} \quad \gamma = \frac{\mathscr{K}}{\mathscr{M}} \tag{48}$$

Solving eqn (46) for p, it is readily found that

$$p = p_0(p_1 \pm \sqrt{p_1^2 + p_2}) \tag{49}$$

According to eqns (46) and (47) the case $p = 0$ corresponds to $R_{TC}(1 - Le) = R^0$, in agreement with the results of eqn (34). However, in general, the constant p is a complex number which can be decomposed as

$$p = q + i\omega \tag{50}$$

where q and ω are its real and imaginary parts, respectively.

It can be easily demonstrated that

$$\left.\begin{array}{l} q = p_0[p_1 + \sqrt{p_1^2 + p_2}] \\ \omega = 0 \end{array}\right\} \quad \text{if } p_1^2 + p_2 \geqslant 0$$
$$\left.\begin{array}{l} q = p_0 p_1 \\ \omega = p_0\sqrt{|p_1^2 + p_2|} \end{array}\right\} \quad \text{if } p_1^2 + p_2 < 0 \tag{51}$$

The marginal state of overstability corresponds to the condition $q = 0$, i.e. $p_1 = 0$. From eqn (47) the resulting overstable critical Rayleigh number, for the onset of oscillatory flows, is given by

$$R_{TC}^{over} = R^0 \frac{(\varepsilon Le + 1)}{Le(\varepsilon - 1)} \tag{52}$$

it marks the transition from the oscillatory to direct convective modes.

This oscillatory regime ($\omega \neq 0$) exists only when the condition $p_1^2 + p_2 < 0$ is satisfied, i.e. $R_{TC}^{over} \leqslant R_T \leqslant R_{TC}^{osc}$, where the value of R_{TC}^{osc} is deduced from the condition $p_1^2 + p_2 = 0$ as

$$R_{TC}^{osc} = R^0 \frac{(\varepsilon Le - 1)}{Le(\varepsilon - 1)^2}[\varepsilon + 1 + 2\sqrt{\varepsilon}] \tag{53}$$

Figure 2 presents series of streamline, isotherm and isoconcentration patterns at the onset of convection as predicted by the linear stability analysis for a square cavity ($A = 1$) and various values of the inclination angle Φ ranging from 0° to 90°. The results obtained for $\Phi = 90°$ will be discussed first. According to the linear stability theory results, it is found that there exists two eigenvalues with the same absolute value but different signs ($\lambda_1 = -\lambda_m$) which corresponds to two mirror image solutions. From eqn (34), it is clear that the sign of R^0 in eqn (35), i.e. $1/\lambda$, depends upon whether Le is greater or smaller than unity. In addition, it is noted that if the eigenvector $\{\psi\}_i$ is a solution of eqn (29) $-\{\psi\}_i$ is also a solution. At the onset of convection, Figs 2(a) and 2(e) show the perturbation fields for $Le < 1$ and $Le > 1$, respectively. As it can be observed from these figures, the flow structures consist of a primary tilted roll cell in the center of the cavity, squeezed by two secondary roll cells, one in the upper right corner and the other one in the bottom left corner for $Le < 1$ (or one in the upper left corner and the other one in the bottom right corner for $Le > 1$). Obviously, the three cells are counter-rotating. As mentioned above, for a given Lewis number, the primary cell can be clockwise and the secondary ones counterclockwise or vise versa. The stability of the two possible solutions will be discussed later.

Upon decreasing progressively the inclination angle Figs 2(b) and 2(c) show the flow patterns obtained at $\Phi = 60°$ and 30°, respectively, when $Le < 1 (R^0 > 0)$. The results indicate that the primary cell grows in size while the two secondary cells dwindle. This behavior is amplified as the value of Φ is reduced down to $\Phi = 0°$, which is presented in Fig. 2(d). For this situation, which corresponds to a cavity heated (destabilizing agent) and salted (stabilizing agent) from below, the resulting flow pattern is a single square cell occupying the entire cavity. This result is in fact similar to the classical Rayleigh–Bénard situation observed in a horizontal porous layer heated from below (see reference [18]). The case with $Le > 1$, i.e. $R^0 < 0$, will be now discussed. As the inclination angle is decreased from 90° to 60° a transition from a three-cells pattern [Fig. 2(e)] to a four-cells pattern [Fig. 2(f)] is observed. In the core of the cavity two large counterrotating cells are squeezed by two secondary circulations. The appearance of very small cells in the upper left and in the lower right corners is also noticed. This formation of a multicellular flow pattern is further favored as the value of Φ is decreased down to $\Phi = 30°$ for which Fig. 2(g) reveals the presence of seven counterrotating cells. Naturally, when $\Phi = 0°$ the system is unconditionally stable since the buoyancy forces, resulting from the stabilizing agent (salt), are predominant over those occasioned by the destabilizing agent (heat).

The numerically determined constant R^0 is presented in Figs 3(a) and 3(b) as a function of the inclination angle of the enclosure Φ for various values of the aspect ratio A. It is seen from the graphs that, for a given value of A, R^0 is an increasing function of Φ. The results obtained for $A = 1$, Fig. 3(a), indicate that when $Le < 1$, $R^0 = 4\pi^2$ at $\Phi = 0°$, in agreement with the analytical solution obtained by Nield [2], and increases monotonously up to infinity as $\Phi \to 180°$ (for which the buoyancy forces induced by the stabilizing agent (heat) overcomes those due to the destabilizing agent (concentration). On the other hand, for $Le > 1$, R^0 increases from $-\infty$ at $\Phi = 0°$ up to $-4\pi^2$ as $\Phi = 180°$. For a given inclination angle Φ, the existence of two solutions, one corresponding to $\lambda_1 (R^0 < 0)$ and the other one to $\lambda_m (R^0 > 0)$ is clearly observed. As discussed above, when $\Phi = 90°$, $\lambda_m = -\lambda_1$ and the two corresponding flow patterns are the mirror image of each other [see Figs 2(a) and 2(e)]. However, in general, for a given inclination angle Φ the two eigenvalues λ_1 and λ_m are not equal yielding two different solutions [see Figs 2(b) and 2(f), for $\Phi = 60°$]. The symmetry of the curves with respect to $\Phi = 90°$ is evident from Figs 3(a) and 3(b). In fact, the present problem is completely described by the values of R^0 predicted in the range $0° \leqslant \Phi \leqslant 90°$ since the value of R^0 obtained for $Le < 1$ and a given Φ, is

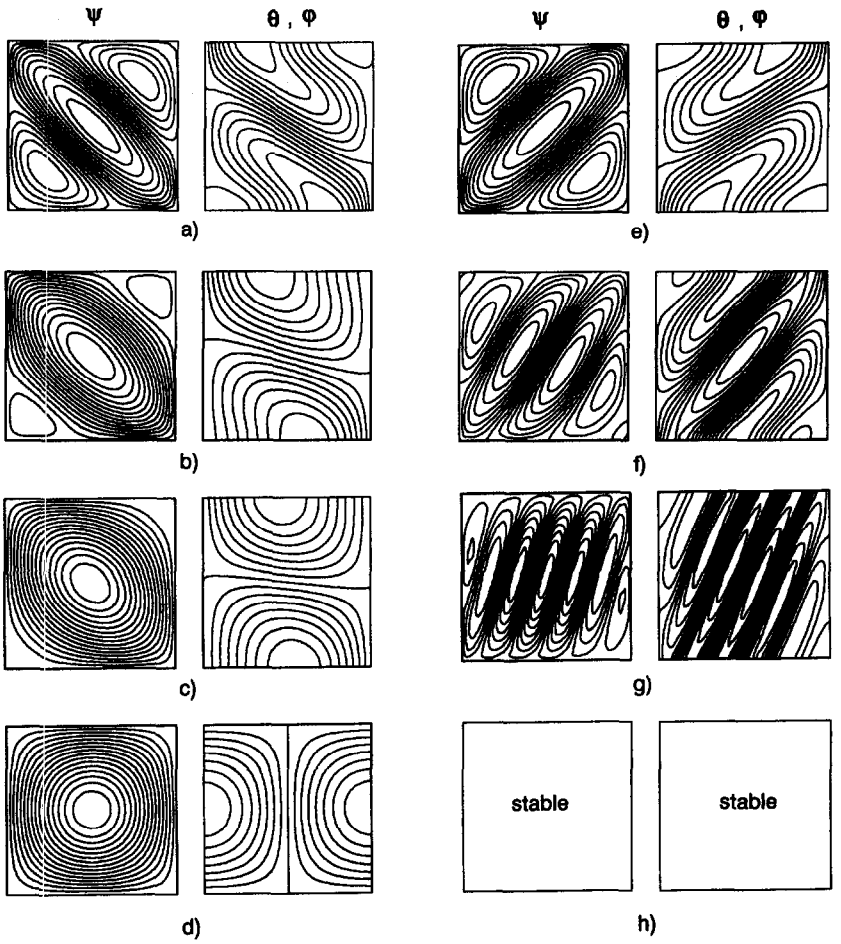

Fig. 2. Streamline, isotherm and isoconcentration patterns at the onset of convection for $Le < 1$; (a) $\Phi = 90°$, $R^0 = 184.0687$; (b) $\Phi = 60°$, $R^0 = 70.3585$; (c) $\Phi = 30°$, $R^0 = 44.9152$, (d) $\Phi = 0°$, $R^0 = 39.4786$ and $Le > 1$; (e) $\Phi = 90°$, $R^0 = -184.0687$; (f) $\Phi = 60°$, $R^0 = -754.9608$; (g) $\Phi = 30°$, $R^0 = -9387.2960$; (h) $\Phi = 0°$, $R^0 = -\infty$.

equal, but of opposite sign, to that obtained for $Le > 1$ and $(180° - \Phi)$. The effect of the aspect ratio of the cavity A on R^0 is illustrated in Fig. 3(b) for $A = 4$ and 0.25, respectively. Naturally, the flow structure obtained for a given value of Φ when $Le < 1$ is a mirror image of that corresponding to $(180° - \Phi)$ and $Le > 1$. From Figs 3(a) and 3(b) it is observed that, for a given Φ, an increase (decrease) in A lowers the critical values $R^0(R^0 \times A^2)$ for the onset of convective motion.

The influence of the aspect ratio A of the cavity on the incipient convection is illustrated on Figs 4(a) and 4(b) for $\Phi = 90°$ and 0°, respectively. The case of a vertical cavity ($\Phi = 90°$) will be discussed first. For a square cavity ($A = 1$), as mentioned earlier, $R^0 = \pm 184.07$ and the flow patterns consist of three counterrotating cells [Figs 2(a)–(e)]. Upon increasing A this flow pattern remains basically unchanged and R^0 decreases monotonously until $A = 2$. At $A \simeq 2.1$ an abrupt change in the variation of R^0 vs A occurs due to the transition from a three cells to a four cells flow. This regime is maintained up to $A \simeq 3$ above which a five cells configuration is reached. This process is continued as the aspect ratio of the cavity is made larger and larger, as illustrated by the eight cells flow pattern depicted in Fig. 4(a) for the case $A = 8$. The numerical results indicate that, for $A \gg 1$, the value of R^0 tends towards a constant which becomes independent of the aspect ratio A ($R^0 = 106.41$ for $A = 10$). In this limit, which corresponds to the case of an infinite vertical porous layer, the flow pattern reveals the formation of a periodical structure consisting of tilted counter-rotating cells (see the streamlines pattern in Fig. 4(a) for $A = 8$). Using periodic boundary conditions ($f(x, y) = f(x, y + A_C)$, where f stands for ψ, θ and ϕ), it was found numerically that the critical wave number A_C and the corresponding critical Rayleigh number are $A_C = 2.503$ and $R^0 = 105.35$ while the tilt angle of the cells with respect to the horizontal plane was $\simeq 65°$ (115°) when $Le < 1$ ($Le > 1$). Similar flow patterns have been reported in the past by Thangan *et al.* [19] while studying double-

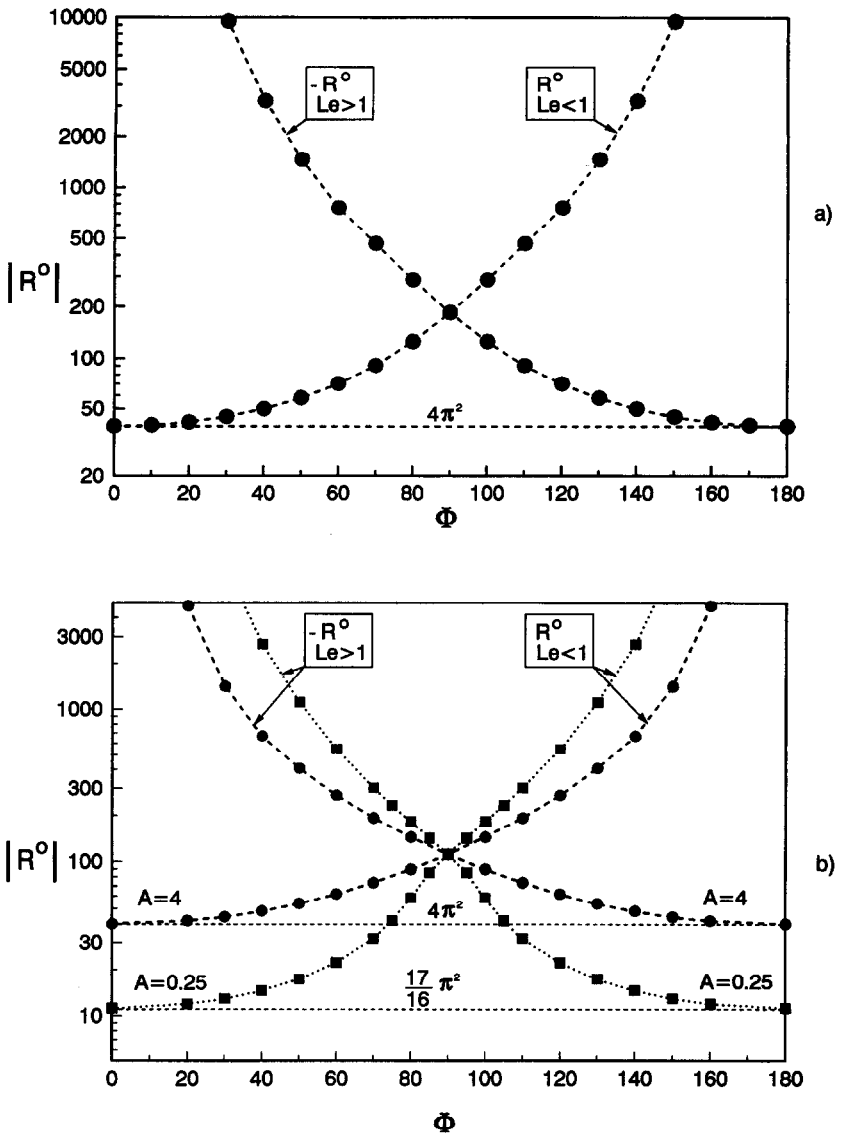

Fig. 3. R^0 as a function of the inclination angle Φ for (a) $A = 1$; and (b) $A = 0.25$ and 4.

diffusive convection in an inclined fluid layer heated differentially from the sides with a stable constant solute gradient imposed in the vertical direction. The case of a shallow cavity ($A < 1$) has also been considered in this study. It is observed from Fig. 4(a) that, upon using a scale $R^0 \times A^2$, the resulting curve for $A \leqslant 1$ is perfectly symmetrical with respect to that for $A \geqslant 1$ (for instance compare the streamline patterns obtained for $A = 1/8$ with those for $A = 8$).

Although the variation of R^0 vs A for the case of an horizontal layer is well known, it is presented here [Fig. 4(b)] for comparison with the vertical layer. The present numerical solution, indicated by solid symbols, are seen to agree well with the analytical solution predicted by Nield [2]. These results apply only for $Le < 1$ when $\Phi = 0°$, for which the destabilizing agent (heat) acts from below, and for $Le > 1$ when $\Phi = 180°$, i.e. when the destabilizing agent (concentration) acts from above. The symmetry with respect to $A = 1$, reported for the vertical layer [Fig. 4(a)], is observed to be destroyed in the case of the horizontal layer. This is due to the fact that for $A < 1$ the only flow configuration possible, independently of the aspect ratio of the cavity, is a single cell (see the streamlines pattern for $A = 1/4$). Thus, the value of $R^0 \times A^2$ decreases monotonously from $4\pi^2$, when $A = 1$ to π^2 as the value of $A \to 0$, this limit being approximately reached by our numerical results when $A < 0.1$. On the other hand, upon increasing A from unity, up to $A = \sqrt{2}$, a one cell mode prevails and R^0 increases from $4\pi^2$ to $9\pi^2/2$. Above $A = \sqrt{2}$, the flow exhibits a two-cells mode and R^0 decreases from $9\pi^2/2$

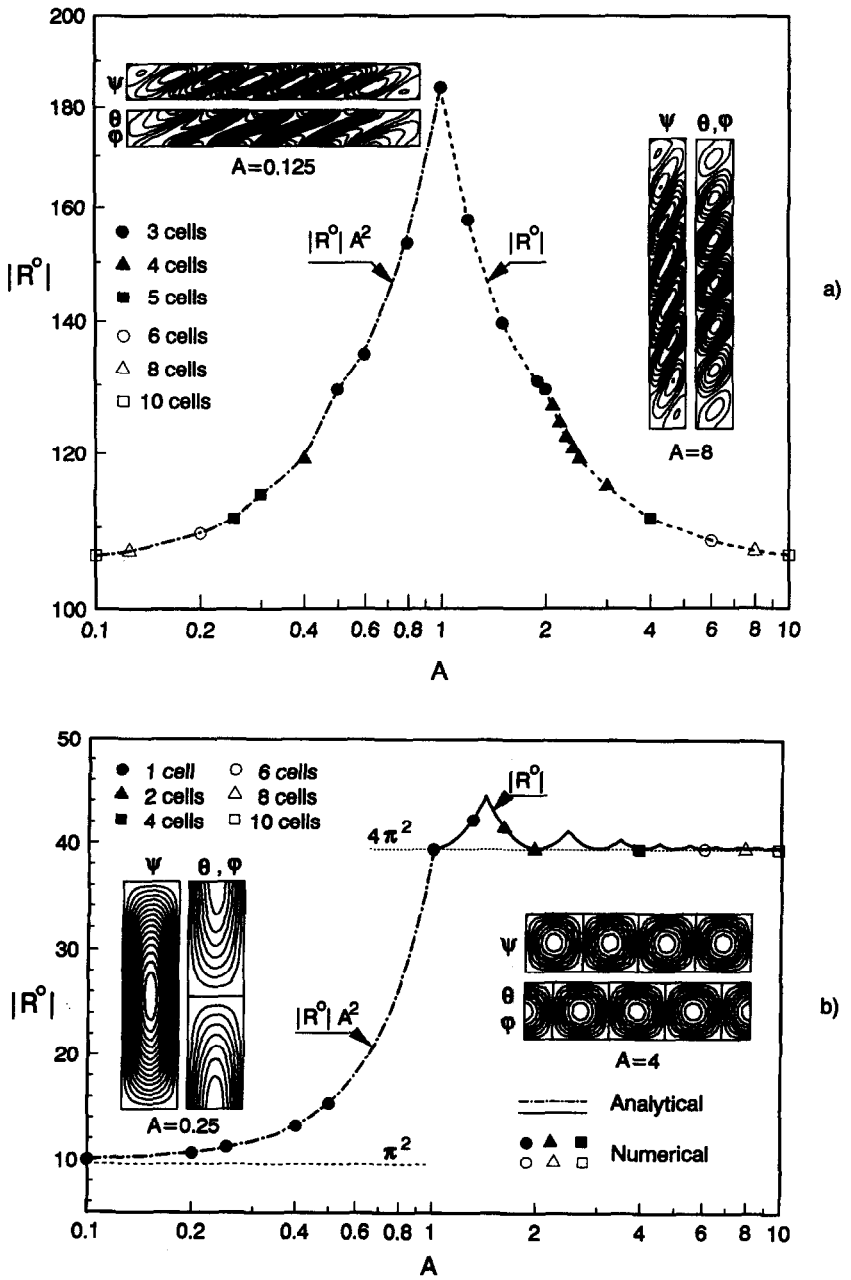

Fig. 4. R^0 as a function of the aspect ratio A (a) $\Phi = 90°$; and (b) $\Phi = 0°$.

to $4\pi^2$ as the value of A increases from $\sqrt{2}$ to 2. This process continues as the value of A is made larger and since the half wave number for the incipient convection in a horizontal layer corresponds to $A = 1$, the value $R^0 = 4\pi^2$ will be reached for all integer multiples of A (i.e. $A = 1, 2, 3, \ldots$). In general, at each value of $A = A_n = \sqrt{n(n+1)}$, the number of cells increases from n to $n+1$ and the corresponding value of the incipient convection is $R^0 = (A_n^2 + n^2)^2 \pi^2 / (A_n^2 n^2)$. An example of this situation is depicted by the numerical results presented in Fig. 4(b) where four cells are obtained for an aspect ratio $A = 4$.

FINITE AMPLITUDE CONVECTION

In order to study the convection flow structures prevailing at Rayleigh numbers above the onset of motion, the full governing eqns (2)–(4) with the associated boundary conditions (7) are solved by a finite-difference method. The stream function, tem-

perature and concentration equations are first discretized according to the well-known central difference scheme for a rectangular mesh size. The discretized equations for Ψ, T and S are then solved at each time step using the last available field values, until convergence to a steady or to a stationary oscillations state is achieved. The energy and concentration equations were solved using the alternating direction implicit method (ADI) of Peaceman and Rachford (Roache [20]). The stream function equation, on the other hand, is solved by the Gauss–Seidel (SOR) iterative scheme at each time step with a relaxation factor of 1.78. A computational grid of 80×80 for $A = 1$ and 80×160 for $A = 4$ was used in this study. This numerical approach was validated by comparing the results obtained with those of Trevisan and Bejan [8]. Grid refinement tests indicate that the heat and mass transfer rates and the stream function values were within 1%. Further details regarding the validation of the numerical simulation may be found in Mamou *et al.* [10, 13].

From the results of the linear stability analysis, presented in the preceding section, it is noticed from eqn (34) that, for $Le = 1$ and $\varepsilon = 1$, the only possible steady state solution is the rest state. This result follows from the fact that, for this situation, the heat and the species diffuse at the same rates, such that the temperature and concentration fields are identical throughout the domain, giving rise to a nil source term in the momentum equation for any value of the Rayleigh number. This point has been discussed in the past by Gobin and Bennacer [21] in the context of the onset of double diffusive natural convection in a vertical layer of binary fluid submitted to equal and opposing horizontal thermal and solutal gradients. In the case of a fluid layer, the equations describing conservation of energy and constituents are the same, when $Le = 1$, such that a rest state will prevail independently of the fact that the steady or the unsteady forms of these equations are considered. On the other hand, in the case of a porous layer it is clear from eqns (3) and (4) that, for $Le = 1$, the transient behavior of the temperature and concentration fields are identical only when the normalized porosity $\varepsilon = \phi/\sigma$, appearing in the first term on the left hand side of eqn (4), is equal to unity. However, in practical situations, since $\phi < \sigma$ it is clear that $0 < \varepsilon < 1$, such that time-dependent flows are possible, even when the Lewis number is equal to unity. For this situation, the solutal diffusing rate is more important that the thermal one and as a result the temperature field becomes different from that of the concentration which gives rise to a non-zero buoyancy force in the momentum equation. In Fig. 5 the time history of the maximum and minimum values of the stream function and the Nusselt and Sherwood numbers are presented for a vertical square cavity ($\Phi = 90°$, $A = 1$) when $R_T = 400$, $Le = 1$ and $\varepsilon = 0.2$. The results clearly indicate the existence of a permanently oscillating flow. To ensure a sustained oscillation the time integration was continued up to $t = 10$. It is observed from the graph that the period of the flow oscillation is about $\tau = 0.06$. Streamlines at the time indicated with (a), (b), (c), (d), (e) and (f), are presented in Fig. 5. A flow reversal, from the thermally dominated structure [Figs 5(a) and 5(f)] to a solutably dominated structure [Fig. 5(e)], is observed to occur in a very short period of time ($\delta t = 0.06$). It is noted that, for the reason discussed above ($\varepsilon \neq 1$), Nu and Sh are different from each other even though the value of Le is equal to unity.

Figure 6 shows the stability diagram, predicted by the linear stability analysis developed in the present study, for the case $\varepsilon = 0.2$. In the graph, the Rayleigh number R_T is normalized with respect to the constant $R^0 (R_T^0 = R_T/|R^0|)$ such that the resulting curves are valid for the general case of rectangular cavity with both arbitrary aspect ratio A and inclination angle Φ (excepted for $\Phi = 0°$ when $Le > 1$ and for $\Phi = 180°$ when $Le < 1$ where the constant R^0 tends towards infinity). All numerical results reported here were obtained for the special case of vertical cavity ($\Phi = 90°$) with an aspect ratio $A = 1$. In the R_T^0–Le plane, three different regions are delineated by the curves resulting from eqns (34), (52) and (53). In region I, below the neutral overstable curve (eqn (34)) and the neutral stable curve (eqn (52)), the system is expected to be stable according to the linear stability theory; the real part q of p (eqn (51)) is negative, such that the flow is decaying with time. Indeed, this prediction is confirmed by the computational data which indicate that in that region, starting with the pure diffusive solution as initial conditions, the fluid remains motionless. To ensure a permanent rest state, the time integration was continued up to $t = 500$.

In region II, above the neutral stability line (eqn (34)) and the neutral oscillating stability line (eqn (53)), a development of instability, via stationary convection, is expected to occur according to the linear stability analysis. All the numerical results obtained in that region demonstrate the existence of a finite amplitude convective mode. As a matter of fact, in region II, the linear stability analysis indicates that the real part q of p [eqn (51)] is positive which means that the flow, independently of the initial conditions, will grow with time. However, this theory predicts only the size of the convective cells and their evolution with time at the very beginning of convection but says nothing about their amplitude or about the behavior of the final converged convective mode (permanent or oscillatory). In other words, the linear stability analysis is valid up to the point where the non-linear terms become strong enough to overcome the linear ones.

Depending upon R_T^0 and Le the numerical results presented in Fig. 6 show that the resulting convective modes can be either stationary or oscillatory. For instance, when $Le = 4$, upon increasing R_T^0 step by step, a transition from the conductive to a steady convective region occurs at $R_T^0 = 1/3$, as predicted by eqn (34). This steady state convective regime prevails approximately up to $R_T^0 = 3$, above which the

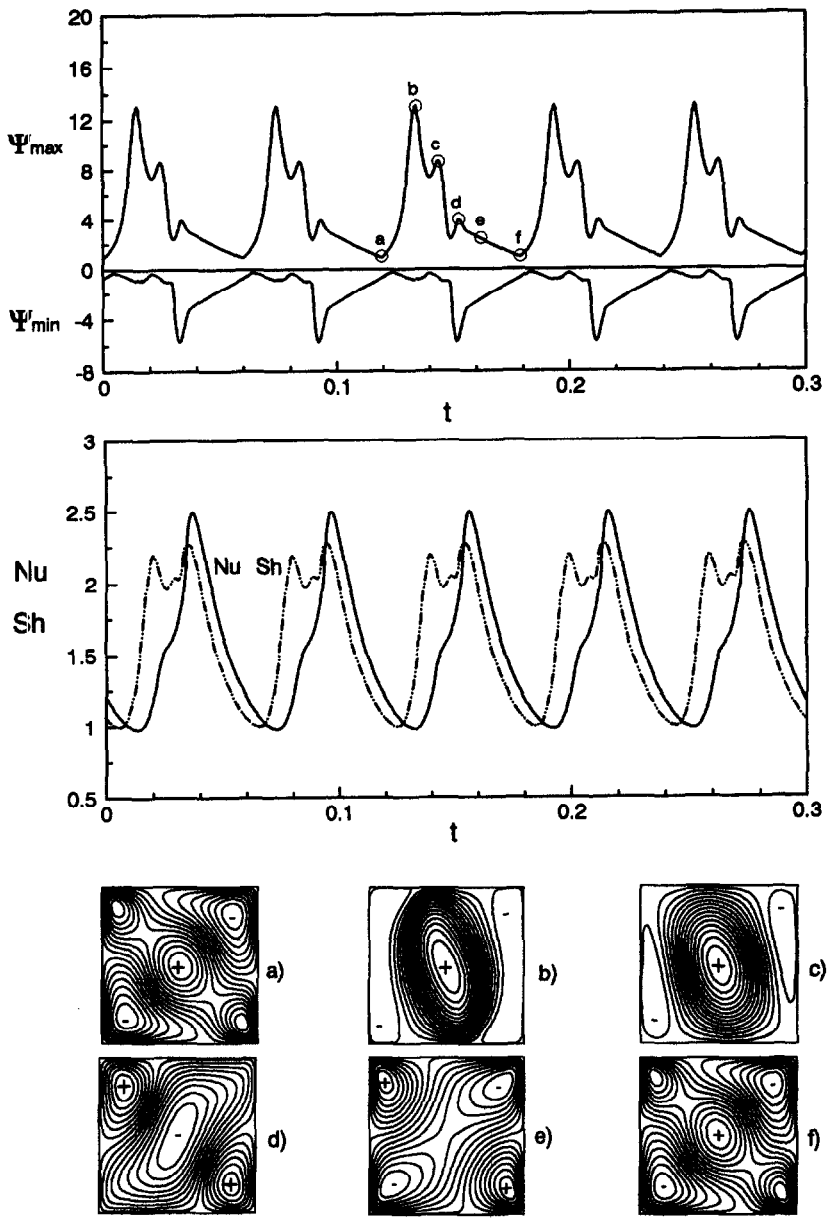

Fig. 5. Time history of Ψ_{max}, Ψ_{min}, Nu and Sh and selected streamline patterns for $R_T = 400$, $A = 1$, $Le = 1$, $\varepsilon = 0.2$ and $\Phi = 90°$.

existence of oscillatory periodic flows is observed. The value of R_T^0 at which transition occurs depends strongly upon the value of Le. Thus, when $Le = 0.2$ a value of R_T^0 as high as $\simeq 7.5$ is required to reach the oscillatory mode. Another way to describe this phenomena is to vary the value of Le for a fixed value of R_T^0. Thus, when $R_T^0 = 2$, upon increasing Le from 0.1 to 0.5 the numerical results indicate that the convective flows remain stationary but the strength of the convection decreases gradually. Passing through the stable region the solution remains purely diffusive up to $Le \simeq 0.71$. Upon increasing further Le the flow becomes oscillatory up to $Le \simeq 2$, above which it is stationary again.

The last region to be discussed is identified by III in Fig. 6. This region is bounded by the lines corresponding to eqns (34), (52) and (53). Here, the linear stability analysis predicts that both real and imaginary parts (q and ω) of p [eqn (51)] are positive. This implies that, as confirmed by the numerical results, when starting the numerical simulations with the pure diffusive solution as an initial condition, the flow, temperature and concentration amplitudes oscillate right at the beginning of convective motion and grow with time. For this situation, the flow structure is multi-cellular and evolves from counter-clockwise to clockwise circulation and vice versa. An example of

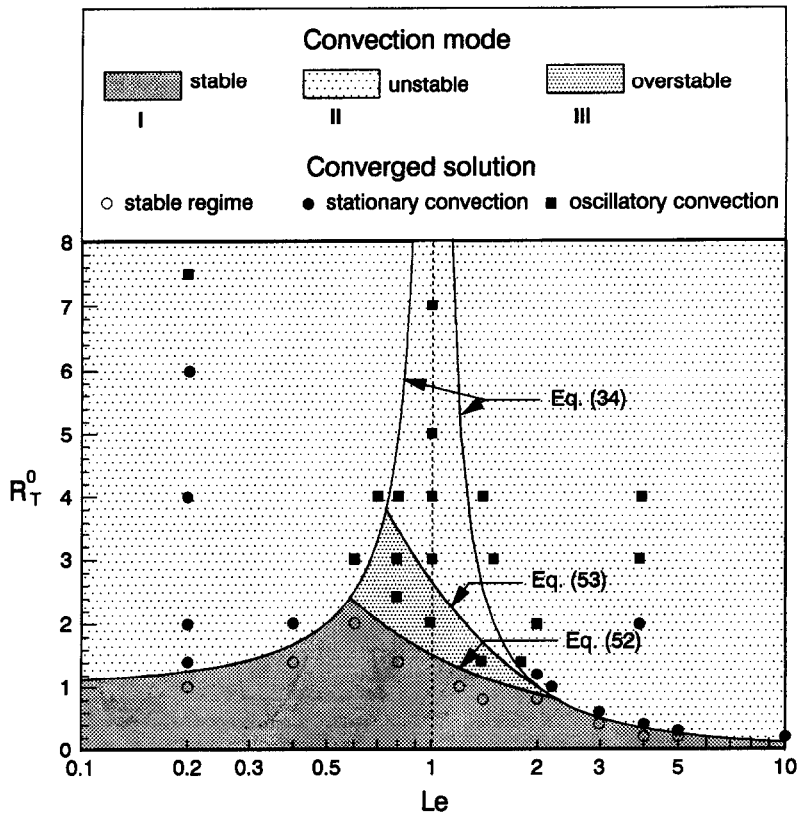

Fig. 6. Stability diagram for $\Phi = 90°$ and $\varepsilon = 0.2$.

this evolution is illustrated in Fig. 5 for $R_T^0 = 2.174$, $Le = 1$ and $\varepsilon = 0.2$. It is worth mentioning that eqns (34), (52) and (53) (for $Le > 1$) intersect at a point having the coordinates

$$Le = \frac{1}{\sqrt{\varepsilon}} \quad R_T^0 = \frac{\sqrt{\varepsilon}}{1-\sqrt{\varepsilon}} \tag{54}$$

Similar expressions can be derived for the intersection between eqns (52) and (34) and between eqns (53) and (34). However, since the resulting equations are lengthy they are not presented here. From these results it can be deduced that the oscillatory region III becomes narrower when $\varepsilon \to 1$ and wider when $\varepsilon \to 0$.

Figures 7(a) and 7(b) illustrate the influence of the Rayleigh number R_T on the maximum and the minimum values of the stream functions Ψ_{max} and Ψ_{min}, respectively, and the average Nusselt and Sherwood numbers, for the case $A = 1$, $\Phi = 90°$, $Le = 10$ and $\varepsilon = 1$. Starting our computation from the purely diffusive solution it was found that this solution can be maintained when R_T was below the critical value $R_{TC} = 20.45$ predicted by eqn (34). However, for $R_T > R_{TC}$, this rest state is unstable, though it continues to be the solution of the governing equations. A stable convective regime bifurcates from the rest state at $R_T = R_{TC}$, for which both *Nu* and *Sh* increase with the Rayleigh number. The resulting supercritical convective regime is characterized, as expected, by symmetrical solutions as exemplified by Figs 7(d) and 7(e) for $R_T = 25$ and 100, respectively. However, upon using a finite amplitude flow as an initial condition, another branch of solutions was found to exist in the range $13 \leqslant R_T \leqslant 35$. This second set of solutions corresponds to non-symmetrical flow patterns as illustrated by Fig. 7(c) for $R_T = 25$. It is noted that this non-symmetrical branch is maintained down to $R_T = 13$, i.e. below $R_{TC} = 20.45$, the critical Rayleigh number value for the onset of supercritical convection. Thus for $13 \leqslant R_T \leqslant 20.45$ two different types of solution are possible, a purely diffusive regime and a subcritical finite amplitude convective regime. The coexistence of the two finite amplitude solutions are also observed to occur in the range $20.45 \leqslant R_T \leqslant 25.5$. In addition, it is worth mentioning that, as discussed earlier, the linear stability analysis predicts that, for $Le = 10$ ($Le > 1$), the flow structure consists of three counterrotating cells [see Fig. 2(e)]. A similar flow structure has been obtained while solving numerically the full system of governing eqns (11)–(13). However, it was found from the numerical solution that only the flow pattern consisting of a primary clockwise rotating cell, at the center of the enclosure, could be sustained. Thus, the other solution predicted by the stability theory, with a primary clockwise rotating circulation, is believed to be unstable.

Figures 8(a) and 8(b) provides another example of

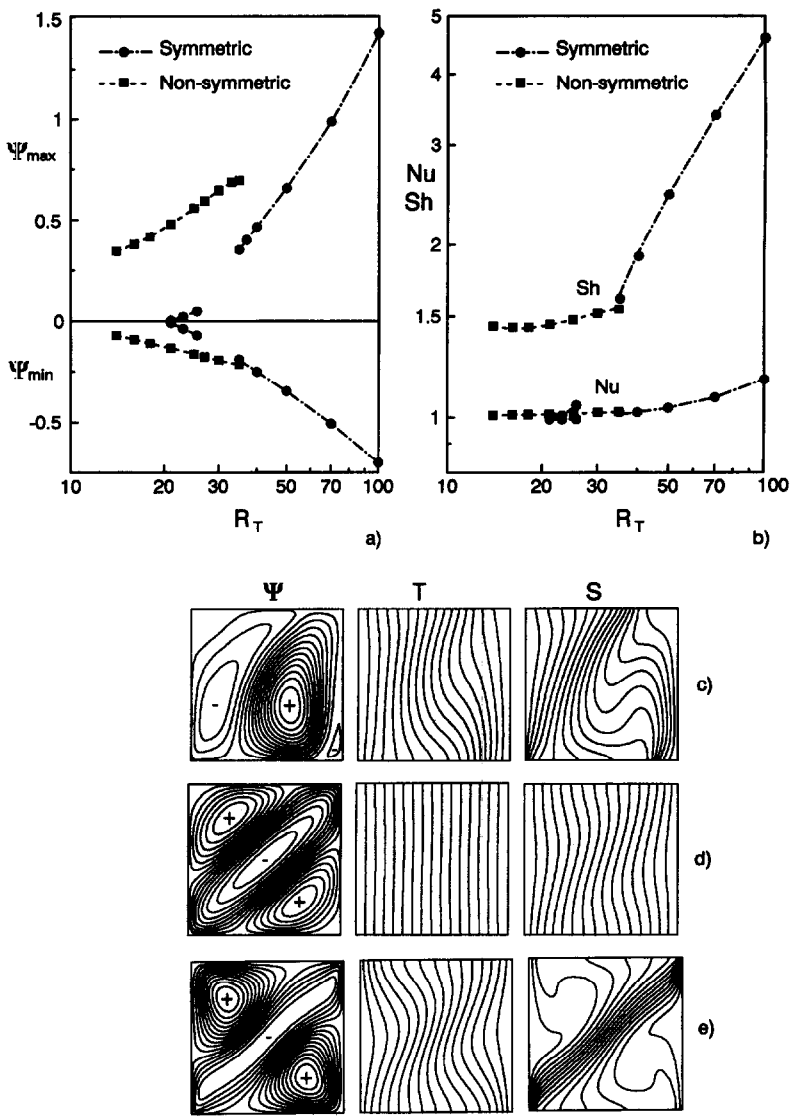

Fig. 7. The effect of R_T on (a) Ψ_{max} and Ψ_{min}; (b) Nu and Sh for $A = 1$, $\Phi = 90°$, $Le = 10$, $\varepsilon = 1$; and streamline, isothermal and isoconcentration patterns for (c) $R_T = 25$, $\Psi_{min} = -0.163$, $\Psi_{max} = 0.555$, $Nu = 1.015$ and $Sh = 1.480$; (d) $R_T = 25$, $\Psi_{min} = -0.063$, $\Psi_{max} = 0.043$, $Nu = 1.001$ and $Sh = 1.047$; and (e) $R_T = 100$, $\Psi_{min} = -0.701$, $\Psi_{max} = 1.423$, $Nu = 1.164$ and $Sh = 4.595$.

the bifurcation diagrams of Ψ_{max}, Ψ_{min}, Nu and Sh for the case $A = 4$, $\Phi = 90°$, $Le = 10$ and $\varepsilon = 1$. Above the critical value $R_{TC} = 12.34$, eqn (34), the numerical results indicate the existence of a single branch corresponding to a symmetrical solution illustrated by Figs 8(c) and 8(d). This convective flow pattern is maintained up to $R_T = 40$ where the flow pattern bifurcates, with discontinuity, on a different branch corresponding to a non-symmetrical solution [see the flow pattern of Fig. 8(e)] that could be maintained up to $R_T = 100$ or more. Also, by decreasing the Raleigh number below the critical value $R_{TC} = 12.34$, it was possible to continue the symmetrical branch down to $R_T = 11.7$. This result indicates here also the existence of a subcritical convective regime.

CONCLUSIONS

A study has been made of the onset of double diffusive natural convection in an inclined porous cavity with equal and opposing buoyancy forces due to the imposition of transverse gradients of heat and solute, applied on two opposing walls of the cavity. The critical stability limit was investigated through a numerical linear stability analysis using the Galerkin finite element method, while a finite difference method was used to simulate convective flows. The main conclusions of the present analysis are:

(1) The marginal states of instability via stationary and oscillatory modes have been determined numerically in terms of the governing parameters of the prob-

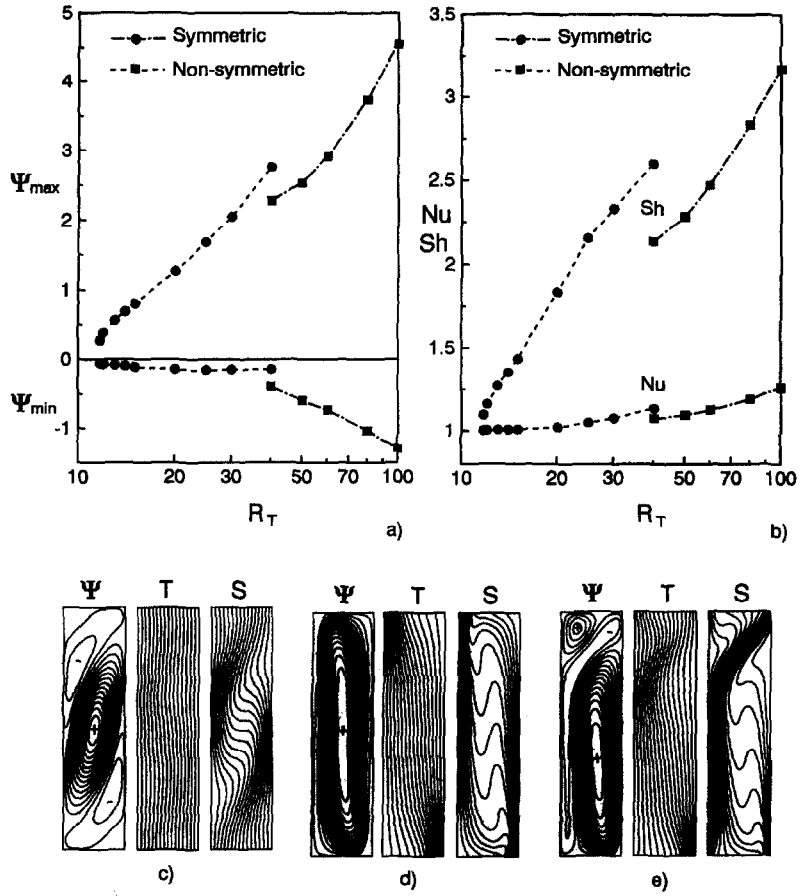

Fig. 8. The effect of R_T on (a) Ψ_{max} and Ψ_{min}; (b) Nu and Sh for $A = 4$, $\Phi = 90°$, $Le = 10$, $\varepsilon = 1$; and streamline, isothermal and isoconcentration patterns for (c) $R_T = 13$, $\Psi_{min} = -0.085$, $\Psi_{max} = 0.560$, $Nu = 1.004$ and $Sh = 1.268$; (d) $R_T = 40$, $\Psi_{min} = -0.143$, $\Psi_{max} = 2.748$, $Nu = 1.135$ and $Sh = 2.595$; and (e) $R_T = 40$, $\Psi_{min} = -0.403$, $\Psi_{max} = 2.273$, $Nu = 1.074$ and $Sh = 2.135$.

lem, namely the inclination angle, the aspect ratio of the cavity, the Lewis number and the normalized porosity of the porous medium.

(2) When the Lewis number is equal to unity, instability via oscillatory convection is the only possible mode since, for this situation, the supercritical Rayleigh number for the onset of convection via stationary convection is infinity. Overstable modes, however, are possible only when the normalized porosity is smaller than unity.

(3) The numerical results, obtained for finite amplitude convection, demonstrate the existence of subcritical convective regimes, the extent of which depends upon the Lewis number, the normalized porosity of the porous medium and the aspect ratio of the cavity. A non-linear stability analysis would be required to study this phenomenon in more detail. Also, for a given set of the governing parameters, transitions between symmetrical and non-symmetrical convective regimes have been observed upon increasing the Rayleigh number. The coexistence of the symmetrical and non-symmetrical solutions was found to occur in a small range of the Rayleigh numbers.

Finally, it is noted that the present linear stability analysis is limited by the assumption of two-dimensional flow and nothing can be inferred about the possible development of three-dimensional instabilities within the range of inclination angle and aspect ratio considered in the present study.

Acknowledgements—This work was supported in part by the Natural Sciences and Engineering Research Council, Canada and jointly by the FCAR, Government of Quebec.

REFERENCES

1. Nield, D. A. and Bejan, A., *Convection of Porous Media*. Springer, 1992.
2. Nield, D. A., Onset of thermohaline convection in a porous medium. *Water Resources*, 1968, **4**, 553–569.
3. Taunton, J., Lightfoot, E. and Green, T., Themohaline instability and salt fingers in a porous medium. *Physics of Fluids*, 1972, **15**, 748–753.
4. Rudraih, N., Shrimani, P. and Friedrich, R., Finite amplitude convection in a two-component fluid porous layer. *International Communication on Heat and Mass Transfer*, 1986, **3**, 587–598.
5. Taslim, M. and Narusawa, U., Binary fluid composition

and double-diffusive convection in a porous medium. *Journal of Heat Transfer*, 1986, **108,** 221–224.
6. Rosenberg, N. and Spera, F., Thermohaline convection in a porous medium heated from below. *International Journal of Heat and Mass Transfer*, 1992, **35,** 1261–1273.
7. Chen, F. and Chen, C., Double-diffusive fingering convection in a porous medium. *Journal of Heat Transfer*, 1993, **36,** 793–897.
8. Trevisan, O. V. and Bejan, A., Mass and heat transfer by natural convection in a vertical slot filled with porous medium. *International Journal of Heat and Mass Transfer*, 1986, **29,** 403–415.
9. Alavyoon, F., On natural convection in vertical porous enclosures due to prescribed fluxes of heat and mass at the vertical boundaries. *International Journal of Heat and Mass Transfer*, 1993, **36,** 2479–2498.
10. Mamou, M., Vasseur, P., Bilgen, E. and Gobin, D., Double-diffusive convection in an inclined slot filled with porous medium. *European Journal of Mechanics/Fluids*, 1995, **14,** 629–652.
11. Lin, D., Unsteady natural convection heat and mass transfer in a saturated porous enclosure. *Wärme- und-stoffübertragung*, 1993, **28,** 49–56.
12. Alavyoon, F. and Masuda, Y., On natural convection in vertical porous enclosures due to opposing fluxes of heat and mass prescribed at the vertical walls. *International Journal of Heat and Mass Transfer*, 1994, **37,** 195–206.
13. Mamou, M., Vasseur, P. and Bilgen, E., Multiple solutions for double-diffusive convection in a vertical porous enclosure. *International Journal of Heat and Mass Transfer*, 1995, **38,** 1787–1798.
14. Mamou, M., Vasseur, P. and Bilgen, E., Thermosolutal convection instability in a vertical porous layer. *Proceedings of the Second International Thermal Energy Congress*, Agadir Maroco, 1995, 463–467.
15. Graham, F. C. and Tinsley, J. O., *Finite Element Fluids Mechanics*. Prentice-Hall. VI, 1986.
16. Norrie, D. H. and De Vries, G., *An Introduction to Finite Element Analysis*. Academic Press Inc., 1978.
17. Huebner, H., Thornton, E. A. and Byrom, T. G., *The Finite Element Method for Engineers*, 3rd edn. Wiley, 1995.
18. Caltagirone, J. P., Thermoconvective instabilities in a horizontal porous layer. *Journal of Fluid Mechanics*, 1975, **7,** 269–287.
19. Thangam, S., Zebib, A. and Chen, C. F., Double diffusive convection in an inclined fluid layer. *Journal of Fluid Mechanics*, 1982, **116,** 363–378.
20. Roache, P. J., *Computational Fluid Dynamics*. Hermose, Albuquerque, 1982.
21. Gobin, D. and Bennacer, R., Double-diffusion in a vertical fluid layer. Onset of the convection regime. *Physics of Fluids*, 1994, **6,** 59–67.